

CrossMark
click for updates

Cite this: DOI: 10.1039/c5ta08574h

First principles study on electrochemical and chemical stability of solid electrolyte–electrode interfaces in all-solid-state Li-ion batteries†

Yizhou Zhu,^a Xingfeng He^a and Yifei Mo^{*ab}

All-solid-state Li-ion batteries based on ceramic solid electrolyte materials are a promising next-generation energy storage technology with high energy density and enhanced cycle life. The poor interfacial conductance is one of the key limitations in enabling all-solid-state Li-ion batteries. However, the origin of this poor conductance has not been understood, and there is limited knowledge about the solid electrolyte–electrode interfaces in all-solid-state Li-ion batteries. In this study, we performed first principles calculations to evaluate the thermodynamics of the interfaces between solid electrolyte and electrode materials and to identify the chemical and electrochemical stabilities of these interfaces. Our computation results reveal that many solid electrolyte–electrode interfaces have limited chemical and electrochemical stability, and that the formation of interphase layers is thermodynamically favorable at these interfaces. These formed interphase layers with different properties significantly affect the electrochemical performance of all-solid-state Li-ion batteries. The mechanisms of applying interfacial coating layers to stabilize the interface and to reduce interfacial resistance are illustrated by our computation. This study demonstrates a computational scheme to evaluate the chemical and electrochemical stability of heterogeneous solid interfaces. The enhanced understanding of the interfacial phenomena provides the strategies of interface engineering to improve performances of all-solid-state Li-ion batteries.

Received 25th October 2015
Accepted 11th December 2015

DOI: 10.1039/c5ta08574h

www.rsc.org/MaterialsA

1. Introduction

All-solid-state Li-ion batteries (ASLiBs) are a promising advancement of the Li-ion battery technology. Using a ceramic solid electrolyte (SE) to replace the organic, flammable polymer electrolyte, which causes notorious safety issues in Li-ion batteries,^{1,2} the ASLiBs benefit from extra safety provided by intrinsically non-flammable ceramic SE materials. In addition, the claimed good stability of SEs may enable Li metal anodes and high voltage cathodes to provide higher energy density, and may suppress the degradation during cycling to achieve good cycle life. For example, a thin-film ASLiB with a Li metal anode and a high-voltage LiNi_{0.5}Mn_{1.5}O₄ cathode was demonstrated for over 10 000 cycles.³ Recent interest in ASLiBs is promoted by the discovery of novel Li ionic conductor materials, such as Li₁₀GeP₂S₁₂ (LGPS)¹ and lithium garnet Li₇La₃Zr₂O₁₂ (LLZO),⁴ with a high Li ionic conductivity of ~1 to 10 mS cm⁻¹, which are

comparable to current organic liquid electrolytes. Despite the high bulk ionic conductivity achieved in the SE materials, the power densities of ASLiBs are still not comparable to those of the ones assembled with organic liquid electrolytes. The high interfacial resistance at the electrolyte–electrode interface is a crucial problem in ASLiBs, limiting the power and rate performances of ASLiBs.² The high interfacial resistance is attributed to poor interfacial contact,⁵ the mechanical failure of the contacts,⁶ interfacial degradation due to mutual diffusion,⁷ or the formation of a lithium-depleted space-charge layer.² The lithium-depleted space-charge layer formed at the interface due to the large chemical potential differences between the sulfide SE and the oxide cathode materials is often blamed as the cause of high interfacial resistance.² The possibility of decomposition at the interfaces is often overlooked since the SEs are claimed to have excellent stability.

However, multiple experimental studies presented the evidence for the interfacial decomposition and the formation of interphase layers at the SE–electrode interfaces. Transmission electron microscopy (TEM) and energy dispersive X-ray (EDX) spectroscopy studies identified interphase layers of tens to a hundred nanometers at the LiCoO₂ electrode–electrolyte interfaces with Li₂S–P₂S₅ (ref. 8) or LLZO.⁷ These interphase layers were attributed to the structural disordering and the mutual diffusion of non-Li elements, such as Co and S, across the interface.

^aDepartment of Materials Science and Engineering, University of Maryland, College Park, MD 20742, USA. E-mail: yfmo@umd.edu

^bUniversity of Maryland Energy Research Center, University of Maryland, College Park, MD 20742, USA

† Electronic supplementary information (ESI) available: The calculated phase equilibria and decomposition energies of the SE materials, the SE–LCO interfaces, and the SE-coating layer interfaces. See DOI: 10.1039/c5ta08574h

Recently, the reactions of Li metal and the SE materials, such as LiPON,⁹ LLTO,¹⁰ and NASICON-type¹¹ SEs, have been demonstrated in *in situ* X-ray photoelectron spectroscopy (XPS) experiments. In addition, recent studies also challenged the claimed wide electrochemical window of the SE materials. The reduction and oxidation of the SE, such as LGPS, have been demonstrated in the cyclic voltammetry (CV) experiments by Han *et al.*¹² and in first principles calculations.^{13,14} The limited electrochemical window of the SEs may also lead to the formation of an interphase layer at the SE–electrode interfaces.¹⁴ These interphase layers have significant effects on the interfacial resistance and the overall performance of the ASLiBs. For example, continued decompositions may lead to interfacial degradation and poor coulombic efficiency of the ASLiBs. In addition, the interphase layers may be poor ionic conductors, which would result in high interfacial resistance.

However, the formation mechanisms of such interphase layers and their effects on the performance of ASLiBs have rarely been discussed. Currently, there is limited knowledge about the formation mechanisms of the interphase layers at the buried SE–electrode interfaces in ASLiBs. The formation of interphase layers in ASLiBs may be caused by three mechanisms:

(1) The reduction or oxidation of SEs under an applied potential due to the limited electrochemical window of the SE materials;

(2) The chemical reactions between the SE and the electrode materials caused by the chemical incompatibility between the SE and the electrodes;

(3) The electrochemical reactions of the SE–electrode interfaces during the voltage cycling of the ASLiBs.

The thermodynamics of these three mechanisms, which correspond to the chemical and electrochemical stability of the interfaces, are well defined. To the best of our knowledge, such thermodynamics information has not been available for the SE and electrode materials in the context of ASLiBs. Understanding the origin of the interfacial decomposition and the formation mechanisms of interphase layers is critical for resolving the issue of high interfacial resistance in ASLiBs and for guiding the development of ASLiBs.

In this study, we employed a computational scheme based on first principles calculations to obtain the thermodynamics of the interfaces between commonly used SEs and electrodes in ASLiBs. Our results confirmed the strong thermodynamic driving force for the decomposition at interfaces in ASLiBs due to the limited electrochemical window of the SE materials and the poor chemical compatibility between the SE and the electrodes. In addition, some of the formed interphases and the applied coating layers were demonstrated to improve the interface stability and the performance of the ASLiBs. The interfaces based on different SEs and interphases were classified into different types, and the strategies to address the interfacial problems were proposed and demonstrated.

2. Methods

All density functional theory (DFT) calculations were performed using the Vienna Ab initio Simulation Package (VASP) within the projector augmented-wave approach. The Perdew–Burke–

Ernzerhof (PBE) generalized gradient approximation (GGA) functional was used. All parameters of DFT calculations, such as the plane wave energy cut-off and *k*-points density, were consistent with the parameters used in the *Materials Project* (MP).¹⁵ The energy correction schemes for oxides, transition metal oxides, and gas molecules such as O₂, N₂, and F₂ were included in the MP.^{16,17}

2.1. Materials systems

The energies for most materials used in our study were obtained from the *Materials Project* (MP) database.²⁶ DFT calculations were only performed for the materials that were not available in the MP database. In this study, we considered five classes of SE materials, which are of great interest to the application of ASLiBs. These SE materials are summarized as follows (Table 1).

(1) Li₁₀GeP₂S₁₂ (LGPS). The ground state structure of the LGPS material from the MP was ordered from the experimental structure.¹ This LGPS structure has an energy above the hull of 21 meV per atom with the phase equilibria of Li₄GeS₄ and Li₃PS₄.¹³ We also considered Li₃PS₄ in comparison with LGPS. The calculated ground state of the Li₃PS₄ phase based on the *Pmn*2₁ γ -phase¹⁸ was added into the Li–P–S composition space.

(2) Lithium garnet Li-ion conductor materials. We investigated the cubic phase of the composition Li₇La₃Zr₂O₁₂ (LLZO). The computational results based on the cubic phase are likely to be applicable to the tetragonal phase, which has similar energies.

(3) Lithium lanthanum titanate perovskite. We investigated the composition Li_{0.33}La_{0.56}TiO₃ (LLTO), which has a high Li ionic conductivity of 1 mS cm^{−1}.²¹

(4) NASICON-type Li ionic conductor. We investigated the composition Li_{1.3}Al_{0.3}Ti_{1.7}(PO₄)₃ (LATP), which has a high Li ionic conductivity of 1 mS cm^{−1}.²³

(5) LiPON, a class of materials based on the chemical formula of Li_xPO_yN_z ($x = 2y + 3z - 5$). The N content is usually in a range from 0.1 to 1.3.²⁷ We studied LiPON compositions Li_{2.88}PO_{3.73}N_{0.14} (LiPON_{0.14}) and Li_{2.98}PO_{3.3}N_{0.46} (LiPON_{0.46}), which are similar to the compositions in the experiments.^{25,28} The crystalline structure Li₂PO₂N,²⁹ a phase missing from the MP database, was added into the Li–P–O–N composition space.

We considered LiCoO₂ (LCO) and Li_{0.5}CoO₂ (L_{0.5}CO) as the discharged and charged states of the cathode material, respectively. We used the layered structure of the L_{0.5}CO composition with the lowest energy (Table 1) to represent delithiated LCO, while the thermodynamically stable phase is the spinel LiCo₂O₄.

2.2. Compositional phase diagram

The compositional phase diagrams were constructed using the *pyratgen* package to evaluate the phase equilibria of a given solid electrolyte or electrode phase with the composition *C*. The phase equilibria were determined by constructing the convex energy hull of all relevant phases in the compositional phase diagram.³⁰ The phase equilibria at the composition *C* corresponding to the energy minimum $E_{\text{eq}}(C)$ were identified by comparing the energy of all relevant phases in their compositional space. The phase stability of the investigated phase was evaluated using the decomposition energy ΔE_{D} ,

Table 1 Summary of the SE and electrode materials investigated in this study^a

Acronym	Composition	Experimental ionic conductivity at room temperature (mS cm ⁻¹)	Crystal structure	<i>E</i> above hull (meV per atom)	Phase equilibria
LGPS	Li ₁₀ GeP ₂ S ₁₂	12 (ref. 1)	MP - 696138 (ref. 1)	21	Li ₃ PS ₄ , Li ₄ GeS ₄
LPS	Li ₃ PS ₄	0.16 (ref. 69)	Ref. 18	0	Li ₃ PS ₄
LLZO	Li ₇ La ₃ Zr ₂ O ₁₂	0.5 (ref. 19)	Ref. 20	7	Li ₂ O, La ₂ O ₃ , Li ₆ Zr ₂ O ₇
LLTO	Li _{0.33} La _{0.56} TiO ₃	1 (ref. 21)	Ref. 22	68	TiO ₂ , Li ₄ Ti ₅ O ₁₂ , La ₂ Ti ₂ O ₇
LATP	Li _{1.3} Al _{0.3} Ti _{1.7} (PO ₄) ₃	1 (ref. 23)	Ref. 24	29	LiTi ₂ (PO ₄) ₃ , Li ₃ PO ₄ , AlPO ₄
LiPON _{0.14}	Li _{2.88} PO _{3.73} N _{0.14}	2 × 10 ⁻³ (ref. 25)	—	0	Li ₂ PO ₂ N, Li ₃ PO ₄ , Li ₂ O
LiPON _{0.46}	Li _{2.98} PO _{3.3} N _{0.46}	3.3 × 10 ⁻³ (ref. 25)	—	0	Li ₂ PO ₂ N, Li ₃ PO ₄ , Li ₂ O
LCO	LiCoO ₂	—	MP - 24850	0	LiCoO ₂
Li _{0.5} CO	Li _{0.5} CoO ₂ (layered)	—	MP - 762036	33	LiCo ₂ O ₄ (spinel)

^a The ionic conductivity is based on the nanoporous β-Li₃PS₄ by Liu *et al.*⁶⁹

$$\Delta E_{\text{D}}(\text{phase}) = E_{\text{eq}}(C) - E(\text{phase}), \quad (1)$$

of a given phase to its phase equilibria. ΔE_{D} is the negative of energy above hull.

2.3. Grand potential phase diagram

Grand potential phase diagrams were constructed to evaluate the stability of a material in equilibrium with an external environment.^{13,30} The grand potential phase diagram identifies the phase equilibria $C_{\text{eq}}(C, \mu_{\text{M}})$ of a given phase with the composition C in equilibrium with the chemical potential μ_{M} of element M. The given phase is stable within a certain range of μ_{M} . Outside the μ_{M} stable range of the phase, the composition of the phase equilibria $C_{\text{eq}}(C, \mu_{\text{M}})$ has a different number of element M from the original composition C , where the number of element M is changed by Δn_{M} . The decomposition reaction energy at the chemical potential μ_{M} is calculated as

$$\Delta E_{\text{D}}^{\text{open}}(\text{phase}, \mu_{\text{M}}) = E_{\text{eq}}(C_{\text{eq}}(C, \mu_{\text{M}})) - E(\text{phase}) - \Delta n_{\text{M}} \cdot \mu_{\text{M}} \quad (2)$$

Using the same scheme as in previous studies,¹³ the electrode potential ϕ was considered as a part of the Li chemical potential μ_{Li} ,

$$\mu_{\text{Li}}(\phi) = \mu_{\text{Li}}^0 - e\phi, \quad (3)$$

where μ_{Li}^0 is the chemical potential of Li metal. In this study, μ_{M} was referenced to the elementary state μ_{M}^0 , and the applied potential ϕ was referenced to Li metal. The electrochemical window of the phase was estimated as the range of ϕ , where the phase is neither oxidized nor reduced. The decomposition reaction energy at applied voltage ϕ was calculated as

$$\Delta E_{\text{D}}^{\text{open}}(\text{phase}, \phi) = \Delta E_{\text{D}}^{\text{open}}(\text{phase}, \mu_{\text{Li}}(\phi)). \quad (4)$$

2.4. Evaluation of chemical stability of interfaces

In this study, we considered the interface as a pseudo-binary³¹ of the solid electrolyte and the electrode, which has a composition

$$C_{\text{interface}}(C_{\text{SE}}, C_{\text{electrode}}, x) = x \cdot C_{\text{SE}} + (1 - x) \cdot C_{\text{electrode}} \quad (5)$$

where C_{SE} and $C_{\text{electrode}}$ are the compositions (normalized to one atom per formula) of SE and electrode materials, respectively, and x is the molar fraction of the SE which varies from 0 to 1. The energy of the interface pseudo-binary

$$E_{\text{interface}}(\text{SE}, \text{electrode}, x) = x \cdot E(\text{SE}) + (1 - x) \cdot E(\text{electrode}) \quad (6)$$

was set to a linear combination of the electrolyte and electrode energies. The decomposition energy of the interface pseudo-binary was calculated similar to eqn (1) as

$$\Delta E_{\text{D}}(\text{SE}, \text{electrode}, x) = E_{\text{eq}}(C_{\text{interface}}(C_{\text{SE}}, C_{\text{electrode}}, x)) - E_{\text{interface}}(\text{SE}, \text{electrode}, x). \quad (7)$$

$\Delta E_{\text{D}}(\text{SE}, \text{electrode}, x)$ includes the decomposition energy ΔE_{D} from eqn (1) if the SE or the electrode is not thermodynamically stable. We defined $\Delta E_{\text{D}, \text{mutual}}$ as the reaction energy between phase equilibria of SE and electrode materials,

$$\begin{aligned} \Delta E_{\text{D}, \text{mutual}}(\text{SE}, \text{electrode}, x) = \\ \Delta E_{\text{D}}(\text{SE}, \text{electrode}, x) - x \cdot \Delta E_{\text{D}}(\text{SE}) - (1 - x) \cdot \Delta E_{\text{D}}(\text{electrode}). \end{aligned} \quad (8)$$

The $\Delta E_{\text{D}, \text{mutual}}$ describes the mutual reaction between SE and electrode materials excluding the decomposition energy ΔE_{D} (eqn (1)) of the SE and electrode. Since the phase equilibria and the reaction energies vary with the pseudo-binary composition, we identified the minimum of the mutual reaction energy,

$$\Delta E_{\text{D}, \text{min}, \text{mutual}}(\text{SE}, \text{electrode}) = \min_{x \in (0,1)} [\Delta E_{\text{D}, \text{mutual}}(\text{SE}, \text{electrode}, x)], \quad (9)$$

which reaches the minimum at $x = x_{\text{m}}$. At the same interface pseudo-binary composition x_{m} , we calculated the total decomposition energy as

$$\Delta E_{\text{D}, \text{min}, \text{total}}(\text{SE}, \text{electrode}) = \Delta E_{\text{D}}(\text{SE}, \text{electrode}, x_{\text{m}}). \quad (10)$$

It is worth noting that the identified x_{m} corresponds to the most exothermic decomposition reactions, while the actual interphase layer may differ from the most favorable thermodynamic phase equilibria and may have a distribution of elemental profile and material compositions across the interfaces (ESI†).

2.5. Evaluation of electrochemical stability of interfaces

The electrochemical stability of the interface was evaluated for the interface pseudo-binary (eqn (5)) using the grand potential phase diagram described in Section 2.3 and the previous study.³¹ The decomposition reaction energy $\Delta E_D^{\text{open}}(\text{SE, electrode}, x, \phi)$ at applied voltage ϕ was calculated as

$$\Delta E_D^{\text{open}}(\text{SE, electrode}, x, \phi) = E_{\text{eq}}(C_{\text{eq}}(C_{\text{interface}}(C_{\text{SE}}, C_{\text{electrode}}, x), \mu_{\text{M}})) - E_{\text{interface}}(\text{SE, electrode}, x) - \Delta n_{\text{Li}} \cdot \mu_{\text{Li}}(\phi). \quad (11)$$

The decomposition reaction energy ΔE_D^{open} was normalized to the number of non-Li atoms because the number of Li changes with the phase equilibria at different applied voltages. Similar to Section 2.4, we defined the mutual reaction energy $\Delta E_{D,\text{mutual}}^{\text{open}}$ as

$$\Delta E_{D,\text{mutual}}^{\text{open}}(\text{SE, electrode}, x, \phi) = \Delta E_D^{\text{open}}(\text{SE, electrode}, x, \phi) - x \cdot \Delta E_D^{\text{open}}(\text{SE}, \phi) - (1 - x) \cdot \Delta E_D^{\text{open}}(\text{electrode}, \phi). \quad (12)$$

to evaluate the reaction energy of the “mutual” reaction between the electrolyte and electrode excluding the decomposition energy $\Delta E_D^{\text{open}}(\text{SE}, \phi)$ and $\Delta E_D^{\text{open}}(\text{electrode}, \phi)$ of the SE and electrode themselves, respectively. Since the phase equilibria and reaction energies are dependent on the pseudo-binary composition, we identified the minimum of the mutual reaction energy at a given applied voltage ϕ as

$$\Delta E_{D,\text{min},\text{mutual}}^{\text{open}}(\text{SE, electrode}, \phi) = \min_{x \in (0,1)} [\Delta E_{D,\text{mutual}}^{\text{open}}(\text{SE, electrode}, x, \phi)] \quad (13)$$

for the mutual reaction between the SE and electrode materials under the applied voltage ϕ , similar to the previous study.³¹ If $\Delta E_{D,\text{min},\text{mutual}}^{\text{open}}(\text{SE, electrode}, \phi) \neq 0$, we calculated the total decomposition reaction energy as

$$\Delta E_{D,\text{min},\text{total}}^{\text{open}}(\text{SE, electrode}, \phi) = \Delta E_{D,\text{min},\text{mutual}}^{\text{open}}(\text{SE, electrode}, x_m(\phi), \phi), \quad (14)$$

where $x_m(\phi)$ is at the minimum point of the mutual reaction energy $\Delta E_{D,\text{min},\text{mutual}}^{\text{open}}$ identified in eqn (13). If $\Delta E_{D,\text{min},\text{mutual}}^{\text{open}}(\text{SE, electrode}, \phi) = 0$, the minimum point x_m of $\Delta E_{D,\text{min},\text{mutual}}^{\text{open}}$ from eqn (9) is used in eqn (14). For the SE-LCO interfaces, we considered the voltage range of ϕ from 2 V to 5 V for Li-ion batteries.

2.6. Equilibrium criteria at the interfaces

In this study, we evaluated the stability of the interfaces on the basis of the following equilibrium criteria. These equilibrium criteria must be satisfied for the interfaces to be thermodynamically stable.

(1) The equilibrium of neutral Li and applied potential across the interfaces and with the external environment. Through this equilibrium, the Li chemical potential μ_{Li} should be equal at the contact points between solid electrolyte and electrode materials. This criterion is equivalent to the equilibrium of the materials

(*i.e.*, the electrochemical stability) against different potentials ϕ (eqn (3)). The equilibration of μ_{Li} and ϕ is facilitated by the good mobility of Li ions in the SE and electrode materials. This equilibrium criterion was investigated in our previous study,¹⁴ and the results are reviewed in Section 3.1.

(2) The equilibrium of neutral non-Li elements across the interfaces. Similar to the equilibrium of Li, the equilibrium of any non-Li element M at the interface requires the equivalence of chemical potential μ_{M} at the contact points between the SE and electrode materials, though non-Li elements such as Co and S are usually not as mobile as Li. In Section 3.2, the analyses were performed regarding the equilibrium of μ_{M} between the SE and LCO.

(3) The full thermodynamic equilibrium of the two materials in contact. This criterion is to evaluate the chemical stability of the interface, which is determined by whether the two materials mixed by a certain ratio (*i.e.*, the interface pseudo-binary defined in Section 2.4) can have an exothermic reaction to form other phases, such as the phase equilibria at the same composition. Such a reaction would not exist if two materials were chemically stable against each other, where the phase equilibria would be equivalent to the two original materials. If the phase equilibria were different from the original interface pseudo-binary, the decomposition energy defined in Section 2.4 was calculated. This criterion considered the full equilibrium of all elements, while only one element is allowed to equilibrate in criteria 1 and 2. We investigated the chemical stability of SE-LCO interfaces in Section 3.3, and the interfaces of the interfacial coating layers were studied in Section 3.5.

(4) The equilibrium of the two materials in contact under an applied potential. This criterion is to evaluate the electrochemical stability of the interface, which is different from the chemical stability in the absence of an applied potential as in criterion 3. We determined the thermodynamic phase equilibria of the interface pseudo-binary (Section 2.5) as a function of the applied potential. Similar to criterion 3, an exothermic reaction to form other phases at the applied potential suggests a thermodynamically favorable decomposition reaction. The electrochemical stability of the SE-LCO interfaces was evaluated using the grand potential phase diagram in Section 3.4.

3. Results

3.1. Electrochemical stability of the solid electrolyte materials

The equilibrium of the SE materials against Li or the applied potential revealed the electrochemical stability of the SE materials and the voltage range where the SE material is stable. For example, Li_2S is stable in the range of 0 to 2.01 V, suggesting its stability against Li metal and the oxidation onset at lower 2 V. However, the sulfide solid electrolyte, such as LGPS, starts to be lithiated and reduced at 1.71 V, which is in agreement with recent CV experiments.¹² The phase equilibria of LGPS at 0 V include Li_3P , Li_2S , and $\text{Li}_{15}\text{Ge}_4$, which were observed in the experiments.¹² Li_3PS_4 has a similar electrochemical window and phase equilibria (Table 2). These phase equilibria at 0 V correspond to the products of the lithiation reaction with Li metal,

which are thermodynamically favorable with reaction energies of -1.23 and -1.42 eV per atom for LGPS and Li_3PS_4 , respectively (Fig. 1b and Table 2). The reduction potential of 1.75 and 2.16 V for oxide SE materials, LLTO and L ATP, respectively, is in good agreement with previous CV experiments, which reported the reduction potential of 1.7 V and 2.4 V, respectively.^{32,33} LiPON compounds show a significantly lower reduction potential at 0.69 V. The phase equilibria at 0 V or against Li metal include Li_3N , Li_2O , and Li_3P , which have been experimentally observed in *in situ* XPS experiments.⁹ Among all the SE materials examined, garnet LLZO shows the lowest reduction potential of as low as 0.05 V and the least favorable decomposition reaction energy of only -0.02 eV per atom at 0 V (Table 2). The low reduction potential and small decomposition energy suggest that LLZO may be kinetically stabilized against Li metal, which is consistent with no reduction at 0 V in many CV experiments.³⁴ A recent report on the reaction of garnet LLZO against Li metal at elevated temperatures may be explained by the thermodynamically favorable reactions between garnet LLZO and Li metal.³⁵ In general, our calculations revealed that most SEs are not intrinsically stable against Li metal and that the reduction of the SE materials is thermodynamically favorable at low potentials.

The SE materials are not thermodynamically stable under high potentials either. Our calculations indicate that the oxidation of LGPS starts at 2.15 V, which is in agreement with the CV experiments.¹² The other sulfide SE Li_3PS_4 exhibits a similar oxidation potential of 2.31 V, and a recent experimental study reported an oxidation potential of 2.6 V.³⁶ The calculated oxidation potential of Li_2S is 2.01 V, which is the voltage for the cathode reaction in lithium–sulfur batteries. The sulfide SEs are oxidized at a similar potential of ~ 2 to 2.5 V. The final phase equilibria of LGPS formed at a voltage higher than 2.31 V (dashed line in Fig. 1a) contain S, P_2S_5 , and GeS_2 (Table 2). The oxide SE materials show a higher oxidation potential than sulfides. The oxidation of LLZO and LLTO starts at 2.91 V and 3.71 V, respectively, and L ATP has the highest anodic limit of 4.31 V. The oxidation of all oxide SEs at high voltages involves O_2 gas release (Table 2 and dashed line in Fig. 1a). The oxidation phase equilibria of LLZO at 5 V include $\text{La}_2\text{Zr}_2\text{O}_7$, which has been observed as one of the decomposition products of LLZO in Li-deficient environments.³⁷ Given the poor kinetics of solid diffusion and gas evolution reaction, significant overpotential is expected for the oxidation reactions of the oxide SE materials. L ATP has the highest oxidation potential and a small decomposition energy of -65 meV per atom at 5 V, indicating its better electrochemical stability than other SE materials at high voltages. Though the oxidation of LiPON started at 1.07 V, the decomposition energy is limited to only a few tens of meV per atom until voltages are higher than 3.8 V and 2.8 V for $\text{LiPON}_{0.14}$ and $\text{LiPON}_{0.46}$, respectively (Fig. 1b). The oxidation reactions at high voltage involve N_2 or O_2 gas release (Table 2 and ESI†) depending on the N and O content in the LiPON composition. Yu *et al.*²⁵ observed the formation of bubbles in the LiPON materials after applying high voltage in experiments. In summary, our calculations found that the thermodynamic intrinsic electrochemical window of most SE materials is

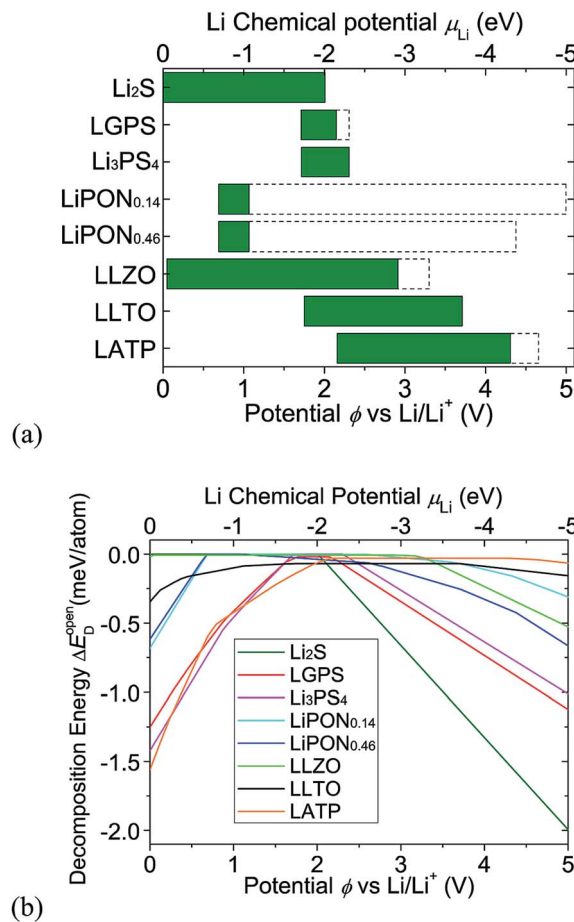


Fig. 1 Electrochemical window (a) and the decomposition energy ΔE_D^{open} (b) of the SE materials. The dashed line in (a) marks the highest equilibrium potential to fully delithiate the material and to form the phase equilibria in Table 2.

significantly narrower than that previously expected and that the reduction and oxidation reactions of some SE materials are highly energetically favorable at low and high potentials, respectively.

3.2. Chemical stability of the solid electrolyte against non-Li elements

In addition to the equilibrium of Li (and ϕ) evaluated in Section 3.1, the equilibrium of non-Li elements such as Co, O and S should also be achieved between the SE and the electrode, though non-Li elements are usually less mobile than Li/Li^+ in the SE and electrode materials. The equilibria evaluated in this section correspond to the chemical stability instead of the electrochemical stability, although the same scheme is used to evaluate the electrochemical stability in Section 3.1. The μ_{O} stability window of LCO and $\text{L}_{0.5}\text{CO}$ electrode materials (Fig. 2a) corresponds to the range of possible μ_{O} values in the cathode material at the discharged and charged states, respectively. The oxide SEs, such as LLZO, LLTO, and L ATP, have the μ_{O} window overlapping with those of LCO and $\text{L}_{0.5}\text{CO}$ (Fig. 2a). This overlapping of the μ_{O} window suggests that a common value of μ_{O} can be achieved across the interface of SE and LCO/ $\text{L}_{0.5}\text{CO}$

Table 2 Electrochemical window and phase equilibria at different potentials ϕ of the SE materials. The decomposition energy ΔE_D^{open} is normalized to the number of atoms in the original composition

	Voltage ϕ (V)/ $-\mu_{\text{Li}}$ (eV)	Corresponding environment	Phase equilibria at ϕ	ΔE_D^{open} (eV per atom)
Li ₂ S	0	Li metal	Li ₂ S (stable)	0
	2.01	Oxidation onset	S	0
	5	Charged at 5 V	S	-1.99
LGPS	0	Li metal	Li ₁₅ Ge ₄ , Li ₃ P, Li ₂ S	-1.25
	1.71	Reduction onset	P, Li ₄ GeS ₄ , Li ₂ S	-0.02
	2.15	Oxidation onset	Li ₃ PS ₄ , GeS ₂ , S	-0.02
	5	Charged at 5 V	GeS ₂ , P ₂ S ₅ , S	-1.12
Li ₃ PS ₄	0	Li metal	Li ₃ P, Li ₂ S	-1.42
	1.71	Reduction onset	P, Li ₂ S	0
	2.31	Oxidation onset	S, P ₂ S ₅	0
	5	Charged at 5 V	S, P ₂ S ₅	-1.01
LiPON _{0.14}	0	Li metal	Li ₃ P, Li ₃ N, Li ₂ O	-0.68
	0.69	Reduction onset	Li ₃ P, Li ₂ PO ₂ N, Li ₂ O	0
	1.07	Oxidation onset	Li ₂ PO ₂ N, Li ₃ PO ₄ , LiN ₃	0
	5	Charged at 5 V	N ₂ O ₅ , P ₂ O ₅ , O ₂	-0.31
	5	Charged at 5 V	Li ₃ P, Li ₃ N, Li ₂ O	-0.62
LiPON _{0.46}	0	Li metal	Li ₃ P, Li ₂ PO ₂ N, Li ₂ O	0
	0.69	Reduction onset	Li ₃ P, Li ₂ PO ₂ N, Li ₂ O	0
	1.07	Oxidation onset	Li ₂ PO ₂ N, Li ₃ PO ₄ , LiN ₃	0
	5	Charged at 5 V	NO ₂ , P ₂ O ₅ , N ₂	-0.66
	5	Charged at 5 V	NO ₂ , P ₂ O ₅ , N ₂	-0.66
LLZO	0	Li metal	Zr, La ₂ O ₃ , Li ₂ O	-0.02
	0.05	Reduction onset	Zr ₃ O, La ₂ O ₃ , Li ₂ O	-0.01
	2.91	Oxidation onset	Li ₂ O ₂ , La ₂ O ₃ , Li ₆ Zr ₂ O ₇	-0.01
	5	Charged at 5 V	O ₂ , La ₂ O ₃ , La ₂ Zr ₂ O ₇	-0.53
	5	Charged at 5 V	O ₂ , La ₂ O ₃ , La ₂ Zr ₂ O ₇	-0.53
LLTO	0	Li metal	Ti ₆ O, La ₂ O ₃ , Li ₂ O	-0.34
	1.75	Reduction onset	Li ₇ Ti ₁₁ O ₂₄ , TiO ₂ , La ₂ Ti ₂ O ₇	-0.07
	3.71	Oxidation onset	O ₂ , TiO ₂ , La ₂ Ti ₂ O ₇	-0.07
	5	Charged at 5 V	O ₂ , TiO ₂ , La ₂ Ti ₂ O ₇	-0.15
	5	Charged at 5 V	O ₂ , TiO ₂ , La ₂ Ti ₂ O ₇	-0.15
LATP	0	Li metal	Ti ₃ P, TiAl, Li ₃ P, Li ₂ O	-1.56
	2.16	Reduction onset	P, LiTiPO ₅ , AlPO ₄ , Li ₃ PO ₄	-0.03
	4.31	Oxidation onset	O ₂ , LiTi ₂ (PO ₄) ₃ , Li ₄ P ₂ O ₇ , AlPO ₄	-0.03
	5	Charged at 5 V	O ₂ , TiP ₂ O ₇ , Ti ₅ (PO ₄) ₄ , AlPO ₄	-0.06
	5	Charged at 5 V	O ₂ , TiP ₂ O ₇ , Ti ₅ (PO ₄) ₄ , AlPO ₄	-0.06

materials where the equilibrium μ_{O} is in the stable window for both materials.

In contrast, the μ_{O} windows of the sulfide SEs, LGPS and Li₃PS₄ have a significant gap with those of LCO and L_{0.5}CO (Fig. 2a). Therefore, no common value of μ_{O} at the interface can simultaneously satisfy the μ_{O} equilibrium criterion between sulfide SEs and LCO materials. The equilibrium μ_{O} would be beyond the stability window of one or both materials, which

would decompose as a result. The μ_{S} stability window of the sulfide SEs does not overlap with that of LCO/L_{0.5}CO either (Fig. 2b). These gaps of μ_{O} and μ_{S} windows suggest that the sulfide SE-LCO interfaces cannot satisfy the criteria (criterion 2 in Section 2.6) for the equilibrium of S and O across the interface. The high μ_{O} of the LCO/L_{0.5}CO tends to oxidize LGPS and Li₃PS₄ into phases including Li₃PO₄ and Li₂SO₄, and the high μ_{S} of sulfide SEs tends to reduce LCO/L_{0.5}CO into phases

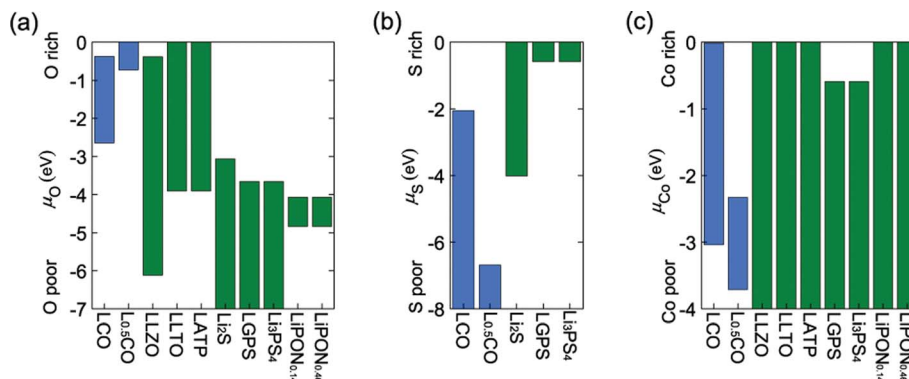


Fig. 2 The stable window of the SE and LCO electrode with respect to the chemical potential of (a) O, (b) S, and (c) Co.

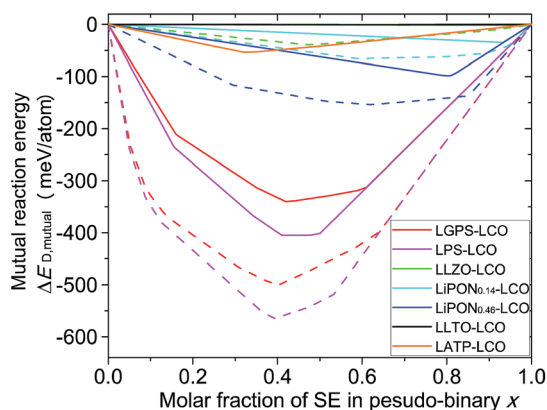


Fig. 3 Calculated mutual reaction energy $\Delta E_{D,mutual}$ of SE–LCO (solid lines) and SE– $L_{0.5}CO$ (dashed lines) interfaces. The mutual reaction energies of LLZO–LCO, LLTO–LCO, LLTO– $L_{0.5}CO$, and LAMP– $L_{0.5}CO$ have zero or near-zero values (minimum values provided in Table 4), which overlap at $\Delta E_{D,mutual} = 0$.

including cobalt sulfides (Fig. 2 and Table 3). The reactions between sulfide electrolytes and LCO cathode materials are highly thermodynamically favorable (Table 3), and the formation of an interphase layer has been reported in several experimental studies.^{8,38} The observed distribution of Co and S across the interface, which was previously interpreted as the mutual diffusion of S and Co,⁸ is likely due to the formation of a cobalt sulfide interphase layer. Similar to sulfides, LiPON also has a μ_O window gap with LCO (Fig. 2a), but its decomposition energy is significantly smaller than that of sulfide SEs (Table 3).

The μ_{Co} stability windows of LCO and $L_{0.5}CO$ overlap with all SEs investigated, suggesting that the equilibrium of Co can be achieved at the interface without going beyond the μ_{Co} window of the SE or LCO materials. This result suggests that the incompatibility between sulfide SEs and LCO mostly originates from the discrepancy of O and S anion chemistries rather than that of Co. The distribution and mutual diffusion of Co across the interfaces observed in the previous EDX experiments⁸ are

likely due to the formation of decomposition interphases such as cobalt sulfides.

3.3. Chemical stability of the SE–LCO interfaces

The equilibria with respect to only one element evaluated in Sections 3.1 and 3.2 correspond to physical situations where only one mobile element reaches equilibrium. Full thermodynamic equilibria (criterion 3 in Section 2.6) evaluated in this section, using the method described in Section 2.4, allow the simultaneous equilibria with respect to all elements and describe the chemical stability of the SE–electrode interfaces. The chemical stability of the interface evaluated in this section is about whether two materials would react exothermically without any applied voltage. This chemical stability of the interface is important for the heat treatment and sintering during the cell preparation. Our calculations found that the interfaces between sulfide SEs and LCO/ $L_{0.5}CO$ are not thermodynamically stable (Fig. 3 and Table 4), in agreement with the results based on the equilibrium of O or S from Section 3.2. The mutual reactions of LGPS with LCO and $L_{0.5}CO$ have favorable decomposition energies $\Delta E_{D,min,mutual}$ of -340 and -499 meV per atom, respectively. Similarly, the decomposition energies of Li_3PS_4 with LCO and $L_{0.5}CO$ are -405 and -564 meV per atom, respectively. The phase equilibria of both interfaces include the formation of Co_9S_8 , Li_2SO_4 , and Li_3PO_4 . The formation of cobalt sulfides at the interface between LCO and the Li_2S – P_2S_5 electrolyte was reported in the experiments.⁸ This reaction corresponds to a valence change of Co from 3+ to 2+. The cobalt sulfide phases with lower valences are known to be electronically conductive,³⁹ which are detrimental to the stability of the interfaces.¹⁴ In addition, the mutual reaction energies of both LGPS and Li_3PS_4 with $L_{0.5}CO$ are lower than those with LCO, indicating a larger thermodynamic driving force for the interfacial decomposition reactions at the charged state of the battery.

The interfaces between the LCO cathode and oxide SEs have significantly better chemical stability with $\Delta E_{D,min,mutual}$ of zero to tens of meV per atom compared to the sulfide electrolytes (Table 4). For example, the minimum reaction energy

Table 3 Phase equilibria of the SE and LCO materials at different chemical potentials of O and S, respectively

	Open element μ_M (eV)	Corresponding environment	Phase equilibria at μ_M	ΔE_D^{open} (eV per atom)
LGPS	$\mu_O = -0.73$	O-Poor limit of $L_{0.5}CO$	GeP_2O_7 , SO_3 , Li_2SO_4	-3.68
	$\mu_O = -2.64$	O-Poor limit of LCO	Li_3PO_4 , S, GeS_2 , Li_2SO_4	-0.46
	$\mu_O = -3.66$	Oxidation onset	Li_4GeS_4 , S, Li_3PO_4	-0.02
Li_3PS_4	$\mu_O = -0.73$	O-Poor limit of $L_{0.5}CO$	$LiPO_3$, SO_3 , Li_2SO_4	-3.73
	$\mu_O = -2.64$	O-Poor limit of LCO	Li_3PO_4 , S	-0.51
	$\mu_O = -3.66$	Oxidation onset	Li_3PO_4 , S	0
LiPON _{0.14}	$\mu_O = -0.73$	O-Poor limit of $L_{0.5}CO$	$LiNO_3$, Li_3PO_4 , $Li_4P_2O_7$	-0.09
	$\mu_O = -2.64$	O-Poor limit of LCO	N_2 , Li_3PO_4 , $Li_4P_2O_7$	-0.02
	$\mu_O = -4.08$	Oxidation onset	Li_2PO_2N , Li_3PO_4 , LiN_3	0
LiPON _{0.46}	$\mu_O = -0.73$	O-poor limit of $L_{0.5}CO$	$LiNO_3$, Li_3PO_4 , $Li_4P_2O_7$	-0.36
	$\mu_O = -2.64$	O-poor limit of LCO	N_2 , Li_3PO_4 , $Li_4P_2O_7$	-0.11
	$\mu_O = -4.08$	Oxidation onset	Li_2PO_2N , Li_3PO_4 , LiN_3	0
LCO	$\mu_S = -0.59$	S-Poor limit of LGPS	Co_9S_8 , Li_2SO_4	-0.28
	$\mu_S = -2.06$	Decomposition onset of LCO	CoO , Li_6CoO_4 , Li_2SO_4	0
	$\mu_S = -6.69$	Decomposition onset of $L_{0.5}CO$	Co_9S_8 , $CoSO_4$, Li_2SO_4	-0.39
$L_{0.5}CO$	$\mu_S = -6.69$	Decomposition onset of $L_{0.5}CO$	Li_2SO_4 , Co_3O_4 , $LiCoO_2$	-0.03

Table 4 The phase equilibria and decomposition energies of the SE–LCO and SE–L_{0.5}CO interfaces

C_{SE}	$C_{electrode}$	x_m	Phase equilibria at x_m	$\Delta E_{D,min,mutual}$ (meV per atom)	$\Delta E_{D,min,total}$ (meV per atom)
LGPS	LCO	0.42	Co ₉ S ₈ , Li ₂ S, Li ₂ SO ₄ , Li ₃ PO ₄ , Li ₄ GeO ₄	−340	−349
	L _{0.5} CO	0.40	Co ₉ S ₈ , Li ₂ S, Li ₂ SO ₄ , Li ₃ PO ₄ , Li ₄ GeO ₄	−499	−527
Li ₃ PS ₄	LCO	0.41	Co ₉ S ₈ , Li ₂ S, Li ₂ SO ₄ , Li ₃ PO ₄	−405	−405
	L _{0.5} CO	0.39	Co ₉ S ₈ , Li ₂ S, Li ₂ SO ₄ , Li ₃ PO ₄	−564	−584
LiPON _{0.14}	LCO	0.93	CoN, Li ₃ PO ₄ , Li ₆ CoO ₄ , N ₂	−35	−35
	L _{0.5} CO	0.59	Co ₃ O ₄ , LCO, LiNO ₃ , Li ₃ PO ₄	−65	−65
LiPON _{0.46}	LCO	0.81	CoN, Li ₂ O, Li ₃ PO ₄	−99	−99
	L _{0.5} CO	0.62	CoO, LCO, Li ₃ PO ₄ , N ₂	−154	−154
LLZO	LCO	0.96	La ₂ O ₃ , Li ₆ Zr ₂ O ₇ , Li ₅ CoO ₄	−1	−8
	L _{0.5} CO	0.47	La ₂ O ₃ , La ₂ Zr ₂ O ₇ , Li ₇ Co ₅ O ₁₂ , O ₂	−39	−60
LLTO	LCO	0.64	Co ₃ O ₄ , La ₂ Ti ₂ O ₇ , Li ₂ TiO ₃ , L _{0.5} CO	−0.5	−44
	L _{0.5} CO	—	LLTO, L _{0.5} CO (stable)	0	—
LATP	LCO	0.32	L _{0.5} CO, Co ₃ O ₄ , Li ₃ PO ₄ , LiAl ₅ O ₈ , TiO ₂	−53	−63
	L _{0.5} CO	—	LATP, L _{0.5} CO (stable)	0	—

$\Delta E_{D,min,mutual}$ of garnet LLZO with LCO and L_{0.5}CO is only −1 and −39 meV per atom, respectively. In addition, LLTO and LATP (Table 4) are thermodynamically stable against the charged state cathode L_{0.5}CO, and their interfaces with LCO have small decomposition energies $\Delta E_{D,min,mutual}$ of only −1 and −53 meV per atom, respectively. The interfacial decomposition reactions may be kinetically inhibited. The good stability of LLTO and LLZO against LCO has been observed in the experiments.^{5,40} However, the sintering of the interfaces at high temperatures may enhance the formation of the interphase layers.⁴¹ The main decomposition phase equilibria of the LLZO–L_{0.5}CO interface include La₂O₃ and La₂Zr₂O₇, O₂ (Table 4), which are similar to the delithiation phase equilibria of garnet LLZO at high voltage (Table 2). The decomposition of the LLZO–L_{0.5}CO interface is mainly due to the delithiation of the LLZO by L_{0.5}CO. Our predicted phase equilibria at the LATP–LCO interface include Co₃O₄, which is also observed as a reaction product at the LCO–LATP interface in an experimental study.⁴² The formation of Li₇Co₅O₁₂ and L_{0.5}CO corresponds to the Co valence increase from 3 + to 4+. The increase of Co valence at oxide SE interfaces is opposite to that at the sulfide SE interfaces, indicating the different nature of interfacial decompositions and the resulting properties between oxide and sulfide SEs. In addition, the decomposition interphase layers including Li₃PO₄ and LiAl₅O₈ can potentially passivate the interface and provide decent Li ionic conductivity across the interface.⁴³ In summary, the oxide SE materials, LLZO, LLTO, and LATP, have significantly better chemical compatibility with the LCO cathode materials compared to sulfide SEs.

LiPON also shows thermodynamically favorable reactions with LCO and L_{0.5}CO (Table 4). The phase equilibria and decomposition energy are highly dependent on the LiPON composition. At a low N content of 0.14, the mutual reaction energy $\Delta E_{D,min,mutual}$ of LiPON is only −35 and −65 meV per atom against LCO and L_{0.5}CO, respectively. At a higher N content of 0.46, the minimum mutual reaction energies with LCO and L_{0.5}CO of −106 and −153 meV per atom, respectively, indicate more favorable decompositions. The LCO chemical compatibility of LiPON is better than that of sulfide SEs but

worse than that of oxide SEs. The formation of an interphase layer and the change of chemical structures at the LiPON/LCO interfaces were observed in *in situ* XPS experiments.⁴⁴ The good compatibility of the LiPON with the LCO cathode material observed in the experiments^{45–48} may be explained by the effect of the interphase layers, including Li₃PO₄, which is a well-known coating material for cathodes^{49–51} and is the dominant decomposition product at the LiPON interfaces.

3.4. Electrochemical stability of the SE–LCO interfaces

In this section, we evaluated the phase equilibria of the SE–LCO interfaces at the applied potential ϕ on the basis of the equilibrium criterion 4 (Section 2.6). These phase equilibria correspond to the interphase evolution, such as lithiation or delithiation, in response to the applied potential, and the interfacial decomposition as described by the reaction energies may become more favorable at certain applied potentials. The interface between LCO and Li₃PS₄ was found to have poor stability over the entire range of the applied voltage from 2 to 5 V. The interfacial mutual reaction energy $\Delta E_{D,min,mutual}^{open}$ is in the range of [−737, −594] meV per atom for LPS from 2 to 5 V (Fig. 4 and Table 5). The total decomposition energy $\Delta E_{D,min,total}^{open}$ of LGPS or Li₃PS₄ reaches −1.27 eV per atom at 5 V (Fig. 4), suggesting highly favorable decompositions at high voltages. Previous experimental studies also reported the formation of interphases of tens of nanometers including cobalt sulfides between LCO and Li₂S–P₂S₅ SE after charging.⁸ The growing differences between $\Delta E_{D,min,mutual}^{open}$ and $\Delta E_{D,min,total}^{open}$ at higher voltages (Fig. 4) are mainly due to the increasing contribution from the delithiation of the SEs to the total decomposition energy $\Delta E_{D,min,total}^{open}$.

The oxide SE–LCO interfaces generally have significantly better stability than the sulfide SEs over the whole voltage range. For example, the LLZO–LCO interface has the minimum interfacial mutual reaction energy $\Delta E_{D,min,mutual}^{open}$ of only −33 meV per atom (Table 5). At high voltage above 4 V, the reaction products, La₂Zr₂O₇ and LaCoO₃, are likely to be poor Li ionic conductor materials. The predicted phase LaCoO₃ was observed

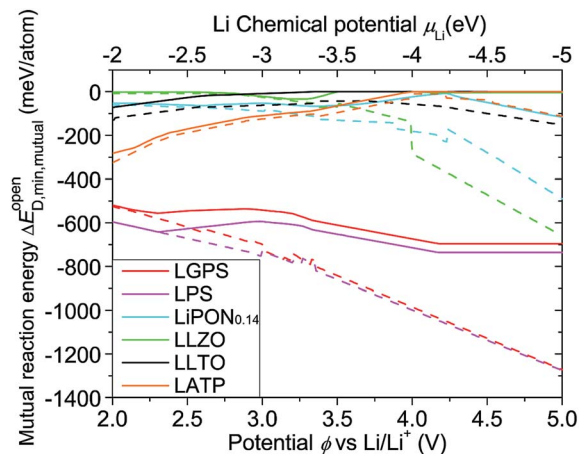


Fig. 4 The mutual reaction energy $\Delta E_{D,\min,\text{mutual}}^{\text{open}}$ (solid lines) and the total reaction energy $\Delta E_{D,\min,\text{total}}^{\text{open}}$ (dashed lines) at the SE–LCO interfaces under applied potential ϕ in a 2–5V range.

experimentally for the LLZO–LCO interface after the heat treatment of over 1000 °C,⁵² which causes Li loss similar to the delithiation at high voltage. In addition, LaCoO_3 may be electronically conductive,⁵³ leading to the formation of thick interphase layers and potential degradation at the interface. However, the final phase equilibria of the interface at high voltage involve O_2 gas release, which is likely to have poor kinetics as in the oxygen evolution reactions in Li–air batteries. A significant amount of overpotential, yielding high oxidation potential observed in many CV experiments, is expected for such oxidation reactions. Similarly, the LCO interfaces with LLTO and LATP show good stability with zero mutual reaction energy $\Delta E_{D,\min,\text{mutual}}^{\text{open}}$ at voltage higher than 3.34 V and 4.53 V, respectively (Fig. 4 and ESI†). The good electrochemical stability of the interfaces between LLTO/LATP and LCO at high voltages may partly be due to high oxidation

potential (anodic limit) of these SEs (Section 3.1) and the good chemical stability between the SEs and LCO (Sections 3.2 and 3.3).

The mutual reaction energy of the $\text{LiPON}_{0.14}$ –LCO interface is comparable to that of oxide SEs, though $\text{LiPON}_{0.14}$ reacts favorably with LCO in the whole 2–5 V range (Fig. 4 and Table 5). The formation of a Li_3PO_4 interphase and the small decomposition energy may explain the widely observed stability of LiPON with LCO.^{45–48} The interfacial reaction between LiPON and LCO also involves N_2 and O_2 gas release. The void formation at the LiPON – LiCoO_2 interface after battery cycling was reported in an *in situ* TEM experimental study.⁴⁷

Our results show that the stability of the interface and the formed phase equilibria are dependent on the applied potential, as the delithiation at high voltages provides an additional thermodynamic driving force for the interfacial decompositions. Among the SE–LCO interfaces investigated, the interfaces of the SEs (such as oxides) that have a good electrochemical window and good chemical stability with the electrode in general show better stability during electrochemical cycling. Therefore, a SE with a wide electrochemical window and good chemical stability with electrodes is desired to achieve intrinsic interface stability during electrochemical cycling. For those SEs (such as sulfides) and interfaces that cannot satisfy the above criteria, an interfacial coating layer material can be applied to resolve the stability problems at the interface.

3.5. Enhanced stability provided by interfacial coating layer materials

The application of coating layer materials to the interfaces between the SEs and cathode materials in ASLiBs has been demonstrated to decrease the interfacial resistance.^{54–60} Using the same computational method as in Section 3.1, we evaluated the electrochemical window of commonly used coating layer materials, such as $\text{Li}_4\text{Ti}_5\text{O}_{12}$,^{54,55} LiTaO_3 ,⁵⁶ LiNbO_3 ,^{57,58} Li_2SiO_3 ,⁵⁹

Table 5 Phase equilibria and decomposition energies of SE–LCO interfaces under applied potential ϕ

Interface	Applied potential ϕ (V)	Phase equilibria at $x = x_m(\phi)$ under ϕ	$\Delta E_{D,\min,\text{mutual}}^{\text{open}}$ (meV per atom)	$\Delta E_{D,\min,\text{total}}^{\text{open}}$ (meV per atom)
Li ₃ PS ₄ –LCO	2.00–2.91	Co ₃ S ₄ , Li ₂ SO ₄ , Li ₃ PO ₄	[−641, −596]	[−737, −596]
	2.91–2.99	Co ₃ S ₄ , Li ₂ SO ₄ , Li ₄ P ₂ O ₇	[−596, −594]	[−750, −737]
	2.99–3.20	Co ₃ S ₄ , Li ₂ SO ₄ , LiCoPO ₄	[−607, −594]	[−779, −730]
	3.20–3.26	Co ₃ S ₄ , Li ₂ SO ₄ , Co ₃ (PO ₄) ₂	[−613, −608]	[−785, −773]
	3.26–5.00	Co ₃ S ₄ , CoSO ₄ , Co ₃ (PO ₄) ₂	[−737, −616]	[−1273, −763]
LLZO–LCO	2.00–2.57	La ₂ O ₃ , Li ₆ Zr ₂ O ₇ , Li ₅ CoO ₄	[−2, −2]	[−9, −9]
	2.57–2.81	La ₂ O ₃ , Li ₆ Zr ₂ O ₇ , Li ₇ Co ₅ O ₁₂	[−7, −2]	[−13, −8]
	2.81–3.50	La ₂ O ₃ , La ₂ Zr ₂ O ₇ , Li ₇ Co ₅ O ₁₂	[−33, −2]	[−72, −11]
	3.50–3.99	La ₂ O ₃ , La ₂ Zr ₂ O ₇ , O ₂ , L _{0.5} CO	0	[−137, −53]
	3.99–5.00	LaCoO ₃ , La ₂ Zr ₂ O ₇ , O ₂	[−5, 0]	[−656, −284]
LiPON _{0.14} –LCO	2.00–2.12	CoN, N ₂ , Li ₃ PO ₄	[−53, −53]	[−55, −55]
	2.12–2.70	CoO, N ₂ , Li ₃ PO ₄	[−64, −53]	[−70, −55]
	2.70–3.01	Co ₃ O ₄ , N ₂ , Li ₃ PO ₄	[−59, −53]	[−84, −70]
	3.01–3.89	Co ₃ O ₄ , LiNO ₃ , Li ₃ PO ₄	[−67, −35]	[−139, −77]
	3.89–4.16	LiCoPO ₄ , LiNO ₃ , Li ₃ PO ₄	[−33, −11]	[−190, −165]
	4.16–4.18	LiCoPO ₄ , LiNO ₃ , Li ₄ P ₂ O ₇	[−9, −9]	[−221, −221]
	4.19–4.23	CoPO ₄ , LiNO ₃ , Li ₄ P ₂ O ₇	[−9, −8]	[−221, −215]
	4.23–4.54	CoPO ₄ , LiNO ₃ , O ₂	[−53, −9]	[−288, −169]
	4.54–5.00	CoPO ₄ , Co(NO ₃) ₄ , O ₂	[−116, −56]	[−482, −294]

and Li_3PO_4 .⁶⁰ The calculations indicate that these coating layer materials have a wide electrochemical window (Fig. 5a) from a reduction potential of less than 2 V to an oxidation potential of ~ 4 V.¹⁴ The highest oxidation potential of the coating layer (dashed line in Fig. 5a) corresponds to the O_2 gas evolution reaction, which is known to yield a high overpotential due to the slow kinetics or poor electron transfer as observed in the oxidation of $\text{Li}_2\text{O}/\text{Li}_2\text{O}_2$ in Li-oxygen batteries.⁶¹ Therefore, nominal oxidation potential of the coating layer is likely to be significantly higher than the equilibrium potential. The wide electrochemical windows suggest that these coating layer materials are likely to be stable at the cathode interfaces during the electrochemical cycling. In addition, the coating layer between the SE-cathode interfaces can achieve the equilibration of μ_{Li} (the equilibrium criteria 1 in Section 2.6) with both the SEs and the cathode. Therefore, the coating layer plays a critical role of passivating and stabilizing the interface by bridging the significant gap of μ_{Li} between the sulfide SE and LCO.¹⁴

The coating layer material lying between the original SE-LCO interfaces forms two interfaces with the SE and LCO, respectively. By applying the same computational scheme as in Section 3.3, we investigated the interfacial chemical compatibility of these two interfaces with the coating layer. The previously demonstrated coating layer materials, such as $\text{Li}_4\text{Ti}_5\text{O}_{12}$, LiTaO_3 , LiNbO_3 , Li_2SiO_3 , and Li_3PO_4 , have excellent chemical stability with the LCO and $\text{L}_{0.5}\text{CO}$ with zero or negligible decomposition energy $\Delta E_{\text{D,min,mutual}}$ (Table 6). In addition, all coating layer materials show better stability with the sulfide SE compared to the original sulfide SE-LCO interfaces, which have an interfacial reaction energy $\Delta E_{\text{D,min,mutual}}$ of ~ -500 meV per atom. As a result, the interface with the coating layer has significantly improved stability, which suppresses the formation of a thick interphase layer. This result of the coating layer was observed as reduced mutual diffusion across the interface in the experiments.^{54,56,59} In addition to stabilizing the interface, the coating layer of only a few nanometers is significantly thinner than the decomposition interphase layer of ~ 10 to 100 nm. The small thickness of the coating layer may significantly reduce the high interfacial resistance caused by the thick decomposition interphase layer.

In addition, we also computationally investigated other compounds (listed in Fig. 5a and Table 6) based on the same cations, such as Ti, Nb, Si, Ta, and P, as potential coating layer materials. All these lithium metal oxide materials have a wide electrochemical window (Fig. 5a). The compounds with a higher Li content generally show lower reduction potential, and the compounds with a lower Li content or higher O content show higher oxidation potential. Most of these compounds have excellent chemical stability against LCO and $\text{L}_{0.5}\text{CO}$ cathode materials with zero or small $\Delta E_{\text{D,min,mutual}}$ (Table 6). All these coating layer materials significantly improve the stability of sulfide SE-LCO interfaces. The chemical stability between LLZO-coating layer interfaces varies significantly with the compositions of the coating layer materials. It is interesting to

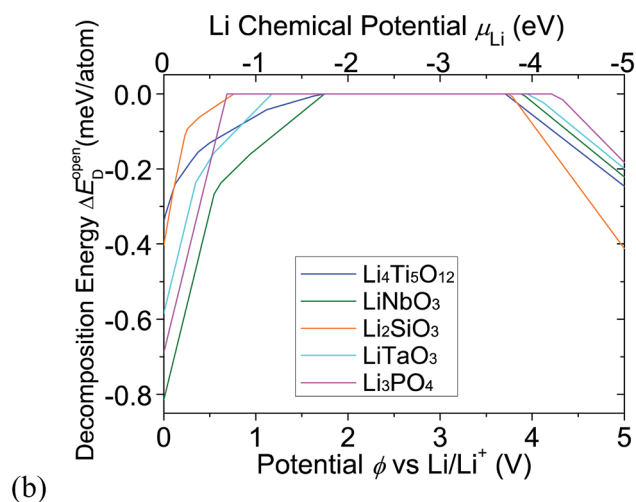
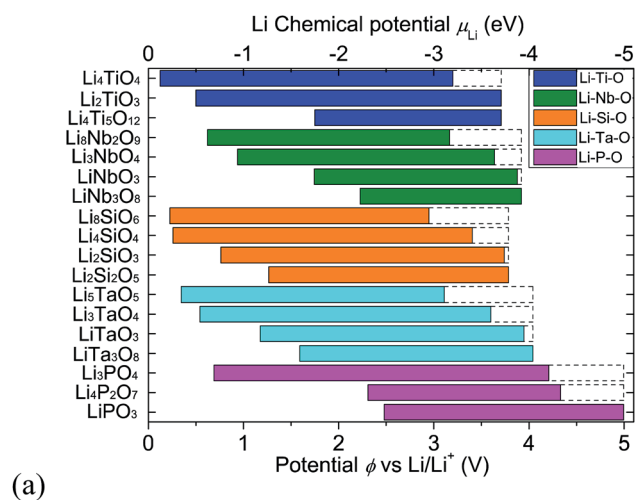


Fig. 5 Electrochemical window (a) and the decomposition energy $\Delta E_{\text{D}}^{\text{open}}$ (b) of the proposed and previously demonstrated coating layer materials applied between SEs and cathode materials. The dashed line in (a) marks the equilibrium voltage to fully delithiate the materials.

Table 6 The mutual reaction energy $\Delta E_{\text{D,min,mutual}}$ (in meV per atom) of the coating layer materials with the SE or LCO materials

	Li_3PS_4	LLZO	LCO	$\text{L}_{0.5}\text{CO}$
Li_4TiO_4	-125	0	0	-30
Li_2TiO_3	-75	-5	0	0
$\text{Li}_4\text{Ti}_5\text{O}_{12}$	-80	-75	-1	0
$\text{Li}_8\text{Nb}_2\text{O}_9$	-147	0	0	-20
Li_3NbO_4	-132	-4	0	0
LiNbO_3	-155	-76	0	0
LiNb_3O_8	-173	-115	-16	0
Li_8SiO_6	-177	0	-3	-50
Li_4SiO_4	-81	-1	0	-12
Li_2SiO_3	-19	-29	0	0
$\text{Li}_2\text{Si}_2\text{O}_5$	-10	-69	-4	0
Li_5TaO_5	-117	0	0	-32
Li_3TaO_4	-64	-3	0	0
LiTaO_3	-49	-68	0	0
LiTa_3O_8	-64	-105	-22	0
Li_3PO_4	0	0	0	0
$\text{Li}_4\text{P}_2\text{O}_7$	-9	-101	-44	-3
LiPO_3	-32	-201	-76	-19

note that the coating layers that are the most stable with sulfide SEs may not necessarily be the most stable ones with LLZO. For example, LiNbO_3 , a demonstrated coating layer for sulfide SEs, is not as stable as Li_3NbO_4 and $\text{Li}_8\text{Nb}_2\text{O}_9$ with LLZO according to the decomposition energy $\Delta E_{D,\text{min,mutual}}$ (Table 6). In the previous study, the application of Nb at the LLZO–LCO interfaces may form amorphous lithium niobates including $\text{Li}_8\text{Nb}_2\text{O}_9$ or Li_3NbO_4 -like phases,⁵⁸ which stabilize the LLZO–LCO interface and hence reduce the interfacial resistance. Similarly, the other Li-rich coating layers, such as Li_4TiO_4 , Li_2TiO_3 , Li_8SiO_6 , Li_4SiO_4 , Li_5TaO_5 , and Li_3TaO_4 , may work better with LLZO than those previously demonstrated for sulfide SEs, such as $\text{Li}_4\text{Ti}_5\text{O}_{12}$, LiTaO_3 , and Li_2SiO_3 .

4. Discussion

Our computational study revealed that the electrochemical and chemical stabilities of the SE–electrode interfaces in the ASLiBs are intrinsically limited. Most SE–electrode interfaces are not thermodynamically stable before, after, and during electrochemical cycling. In particular, the sulfide SEs are neither chemically nor electrochemically stable against the LCO cathode, due to the anion chemical potential discrepancy between sulfide SEs and LCO. The oxide SEs have significantly better chemical and electrochemical stabilities with the LCO cathode than sulfide SEs. The interfacial reactions between oxide SEs and LCO, though may be kinetically limited, are also thermodynamically favorable, suggesting potential interfacial degradations after thermal processing or during battery cycling. These results about the interfacial thermodynamics suggest the ubiquitous formation of the interphase layers at the SE–electrode interfaces, which has significant implications for the research and development of the ASLiBs. The properties of these interphase layers would be critical to the performance of the ASLiBs. In particular, the distinctive chemical nature of sulfide and oxide SEs leads to very different interphase properties for the SE–LCO cathode interfaces and hence requires different interfacial engineering strategies. Following the definitions by Wenzel *et al.*,¹⁰ we distinguish three different types of interfaces based on the interface stability and interphase properties.

Type 1 interface – stable interfaces with no decomposition interphase layer. Type 1 interfaces are either thermodynamically intrinsically stable or kinetically stabilized over the cycling voltage range. Type 1 interfaces do not have an interphase layer between the SE and electrode, and are expected to have decent interfacial ionic conductivity, because both the SE and the electrode are good Li ionic conductors. However, our thermodynamic analyses demonstrated that few SE materials have thermodynamically intrinsic stabilities against Li metal anodes or high-voltage cathodes, or over the entire range of cycling voltages. Among five classes of SE materials investigated, LLTO and LATP have the best electrochemical stability against LCO cathode materials at high voltages, and LLZO has the best stability against Li metal. Some oxide SEs may form kinetically stabilized Type 1 interfaces with the electrode materials,^{5,40} though these Type 1 interfaces may still degrade and convert to

other types during sintering or electrochemical cycling due to the limited thermodynamic stability. Type 1 interfaces require SEs with a wide electrochemical window and good chemical compatibility with the electrode materials. Since the electrochemical window of the SEs and the chemical compatibility of the SE–electrode interfaces are limited, it is unrealistic to have a SE with Type 1 interfaces against both Li metal anodes and high-voltage cathodes.

Type 2 interface – interfaces formed with interphase layers that are mixed ionic and electronic conductors (MIECs). The formation of the interphase layer between the SE and the electrode is expected for most Li–SE and SE–LCO interfaces as suggested by the interfacial thermodynamics from our computation. The electronic conductivity of the interphase, regardless of specific electronic conductive mechanisms, determines whether the interface is Type 2 or Type 3. If the formed interphase is a MIEC, the simultaneous transport of Li ions and electrons would enable continued decomposition reactions that are thermodynamically favorable. Therefore, the MIEC interphases cannot provide essential passivation at the interface.¹⁴ The examples of Type 2 interfaces include the Li–LGPS and Li–LLTO interfaces, which formed interphases including the electron-conducting Li–Ge alloys and lithium titanates, respectively. The formation of Type 2 interfaces explains the Li reduction of the LGPS and LLTO materials observed in the experiments.^{12,32} The continued decomposition may result in poor coulombic efficiency in ASLiBs. Therefore, Type 2 interfaces, which may cause continued interfacial degradation and high interfacial resistance, should be avoided in the ASLiBs. The application of artificial coating layers can be used to engineer Type 2 interfaces into Type 3 interfaces.

Type 3 interface – interfaces formed with a stable solid-electrolyte interphase (SEI). In contrast to Type 2 interfaces, the interphase layers in Type 3 interfaces are electronically insulating and are stable during the electrochemical cycling, acting as a stable SEI at the SE–electrode interfaces. Type 3 interfaces with spontaneously formed SEIs have self-limiting interfacial degradation. The SEIs passivate the SE materials and stop the continued decomposition into the bulk of the SE.¹⁴ The Li–LiPON interface is Type 3, where the formed interphases containing Li_2O , Li_3N , and Li_3P are electronically insulating.^{9,14} In addition, the interphase decomposition layer, including fast Li-ion conducting Li_3N and Li_3P ,^{63,64} is likely to yield low interfacial resistance. The interfacial resistance of Type 3 interfaces is highly dependent on the ionic conductivity of the SEIs. The Li–LiPON interface is an ideal Type 3 interface which has spontaneously formed SEIs with high ionic conductivity. For those Type 3 interfaces with poor Li-ion conducting SEIs, the application of a coating layer with good ionic conductivity as the artificial SEI may resolve the high resistance problem of the spontaneously formed SEIs.

We summarize the categorization of different combinations of SEs and electrode materials into the defined interface types. Our discussion focuses on Li metal anode and LCO cathode materials (similar results are expected for other transition metal oxide cathodes), which are often desired for the ASLiBs. For Li–SE interfaces, Type 1 interfaces are rare due to the strong

thermodynamic driving force for Li metal to reduce the SE. The Li–LLZO interface may be Type 1 as a result of kinetic stabilization and small thermodynamic driving force for Li reduction. The high temperature treatment may facilitate the Li reduction of LLZO.³⁵ The Li–LiPON and Li–Li₃PS₄ are typical Type 3 interfaces, where the passivation layers of high Li ionic conductivity and poor electronic conductivity are formed. The Li–LGPS, Li–LLTO, and Li–LATP are typical Type 2 interfaces, where significant reduction of the SE is observed. Cations, such as Ti and Ge, in SEs would facilitate the formation of the Type 2 interfaces, because of the formation of the electron conducting interphase layers after Li reduction. Therefore, the use of these cations should be avoided in the design of SE materials for Li metal compatibility. In contrast, anion mixing should be a viable strategy for the SE material design to simultaneously improve stability and Li ionic conductivity. LiPON is a successful case of using oxynitride to achieve good stability and Li ionic conductivity. Similar successes have been demonstrated in the doping of Li₃PS₄ with halides, such as LiCl and LiI.^{65,66} Similarly, we expect some oxysulfide compounds as promising SEs.

The interfaces between the SE and cathode, such as LCO, are more complicated, due to a large number of elements involved and a wide range of Li chemical potentials from the charged to the discharged states of the battery. The sulfide SE–LCO interfaces may also be partially Type 2, because the interphases include the cobalt sulfide binaries such as Co₉S₈ or Co₃S₄, which are electronically conductive.^{39,62} This formation of MIEC interphases may explain the large thickness of the interphase layers of 10–100 nanometers observed at these sulfide–LCO interfaces.⁸ Thick interphase layers generally result in a high interfacial resistance. However, the decomposition does not happen to the entire bulk of SEs due to the limited diffusion of Co and the drop of the Co content inside the SEs. The part of the interphase close to SE has a low content of Co sulfides and is still passivating (Type 3), which stops the further growth of the interphase layers. The variation of the interphase composition across the interface has been observed in our computation (ESI[†]) and the EDX experiments.^{38,39} Therefore, the sulfide SE–cathode interface is not purely Type 2 (as in Li–LLTO) but rather a mixture of Type 2 and Type 3. Having some Type 2 features inside the interphase may have negative impact on the electrochemical performance of the ASLiBs. The enabled transport of both Li⁺ and e[−] through the MIEC interphase would facilitate the electrochemical cycling of these interphase layers during cycling voltages (as predicted in Section 3.4). Active electrochemical cycling of these interphase layers may facilitate the growth of the decomposition interphase layers and may lead to a repetitive volume change and the failure of the mechanical contact as a result of cyclic lithiation and delithiation.¹² Such interfacial phenomenon may explain the poor cyclability of the ASLiBs. Therefore, the key problem of sulfide SE–LCO interfaces is the poor stability, which leads to thick interphase layers, high interfacial resistance, and degradation over cycling. Therefore, the application of the coating layer at these interfaces is the corresponding strategy to address the stability issue by turning the interfaces into a desired Type 3 interface with a thin thickness interphase layer and improved

interfacial conductivity. The coating layers serve as artificial SEIs to stabilize the interface and to resolve the issue of poor interfacial conductivity.

In general, we found that the oxide SE and LCO interfaces may be Type 1 or Type 3. In particular, LLTO–L_{0.5}CO and LATP–L_{0.5}CO are thermodynamically stable as Type 1, and other oxide SE–LCO interfaces may be kinetically stabilized as Type 1. After the thermodynamically favorable decomposition between these materials, some oxide SE–LCO interfaces may turn into Type 3, because the formed interphases are mostly electronically insulating at high voltages. However, such interphases and formed SEI layers in some Type 3 oxide SE–cathode interfaces may have poor Li ionic conductivity, since most of the equilibrium phases have low or zero Li content as a result of the delithiation. For example, the spontaneous decomposition interphases, such as La₂Zr₂O₇, of the LLZO–LCO interface are likely to be poor Li ion conductors. For these Type 3 interfaces, the key issue is not poor interfacial stability but the low ionic conductivity of the formed interphase layers. Therefore, interfacial engineering for the aforementioned Type 3 interfaces is also necessary to improve interfacial ionic conductivity. The increased interfacial conductivity after applying a lithium niobate interphase layer in the previous study³⁸ may be due to the higher ionic conductivity of the coating layer than that of the spontaneous decomposition interphase. In addition, the soft and ductile Nb metal may enhance the wetting and may promote the interfacial contact between the LLZO and LCO. As illustrated above, the categorization of different types of interfaces is critical to understand the problems at the interfaces and to apply corresponding interfacial engineering, which is the key to achieve desired interfacial properties and to improve electrochemical performance of ASLiBs.

Our scheme is only based on the thermodynamics of the two materials in contact and the applied external environments, so the kinetics of the equilibrium processes are not considered. It is possible that some predicted reactions may be kinetically inhibited and that a metastable equilibrium state may be reached. Therefore, the actual formed interphase may be different from the thermodynamic phase equilibria identified in the computation. In addition, the evaluation of the interfacial stability is based on the equilibria of neutral elements between the two materials in contact. These equilibria are necessary conditions for the equilibrium of two materials at the interfaces. In addition to the equilibrium of neutral elements, all charged carriers such as Li⁺ and e[−] also need to reach equilibria at the interfaces.⁶⁷ The equilibria of all the charged carriers redistributing at the interface would result in the formation of space-charge layers and electrostatic polarizations at the interfaces. Our scheme is based on the equilibrium conditions that are independent of the interfacial electrostatic polarization, and uses the energies of bulk materials. The structural disordering, crystallography terminations of the interfaces, and the complex microstructures, which may also affect the aforementioned equilibria, are not explicitly considered in our calculation scheme. These atomistic and microstructural features may also change the electronic conductivity of the interphase and the corresponding interface types. Nevertheless, the computational

scheme demonstrated in this study is a good proxy of interface stability and provides valuable thermodynamic information about the chemical and electrochemical stability of interfaces in good agreement with experiments. This computational scheme can be generalized to any heterogeneous interface in solid-state devices, where the interfacial stability is of crucial importance. The bulk phase thermodynamic data for this computational scheme are available and accessible from the computational database infrastructure such as the *Materials Project*.²⁶ The scheme relies on such databases to provide comprehensive phase diagrams to identify the phase equilibria. The phase diagrams might be incomprehensive if some phases that exist in nature were missing from the database in the relevant compositional space. Such a situation is more likely during the evaluation of previously less studied compositional space or high-dimensional phase diagrams, where some multi-component phases may have not been identified. In this study, we added in some known phases, such as Li_3PS_4 and $\text{Li}_2\text{PO}_2\text{N}$, into the relevant compositional spaces. In addition, our computation is limited by the accuracy of the energies provided by the DFT⁶⁸ and the approximations in our proposed scheme. For example, the energies are based on 0 K DFT calculations, so the contribution of entropy to the free energy was neglected. This assumption may have little effect on the conclusions of our computation, because the entropy differences between solid-state phases are usually small.

Conclusion

In this study, we applied first principles calculations to evaluate the thermodynamics of the chemical and electrochemical stability of the SE–electrode interfaces in ASLiBs. Most SE materials have a limited electrochemical window, and many SE–electrode interfaces have limited chemical and electrochemical stability. The computational results suggest thermodynamically favorable, ubiquitous formation of the interphase layer at SE–electrode interfaces. Different types of interfaces form interphase layers with different properties. Some interfaces with poor stability may cause interfacial degradation and high interfacial resistance, significantly impacting the performance of ASLiBs. Interface engineering strategies of applying artificial coating layers were proposed to improve the interfacial stability and electrochemical performance of ASLiBs. Our results suggest the critical roles of electrolyte–electrode interphases in the electrochemical performance of ASLiBs and the importance of interface engineering in the design of ASLiBs.

Acknowledgements

We thank Prof. Chunsheng Wang and Fudong Han for helpful discussion. This work was supported by the U.S. Department of Energy, Office of Energy Efficiency and Renewable Energy, under award No. DE-EE0006860. This research used computational facilities from the University of Maryland super-computing resources and from the Extreme Science and Engineering Discovery Environment (XSEDE) supported by National Science Foundation award No. TG-DMR130142.

References

- 1 N. Kamaya, K. Homma, Y. Yamakawa, M. Hirayama, R. Kanno, M. Yonemura, T. Kamiyama, Y. Kato, S. Hama, K. Kawamoto and A. Mitsui, *Nat. Mater.*, 2011, **10**, 682–686.
- 2 K. Takada, *Acta Mater.*, 2013, **61**, 759–770.
- 3 J. Li, C. Ma, M. Chi, C. Liang and N. J. Dudney, *Adv. Energy Mater.*, 2015, **5**, 1401408.
- 4 V. Thangadurai, D. Pinzaru, S. Narayanan and A. K. Baral, *J. Phys. Chem. Lett.*, 2015, **6**, 292–299.
- 5 S. Ohta, T. Kobayashi, J. Seki and T. Asaoka, *J. Power Sources*, 2012, **202**, 332–335.
- 6 Y. J. Nam, S.-J. Cho, D. Y. Oh, J.-M. Lim, S. Y. Kim, J. H. Song, Y.-G. Lee, S.-Y. Lee and Y. S. Jung, *Nano Lett.*, 2015, **15**, 3317–3323.
- 7 K. H. Kim, Y. Iriyama, K. Yamamoto, S. Kumazaki, T. Asaka, K. Tanabe, C. A. J. Fisher, T. Hirayama, R. Murugan and Z. Ogumi, *J. Power Sources*, 2011, **196**, 764–767.
- 8 A. Sakuda, A. Hayashi and M. Tatsumisago, *Chem. Mater.*, 2010, **22**, 949–956.
- 9 A. Schwöbel, R. Hausbrand and W. Jaegermann, *Solid State Ionics*, 2015, **273**, 51–54.
- 10 S. Wenzel, T. Leichtweiss, D. Krüger, J. Sann and J. Janek, *Solid State Ionics*, 2015, **278**, 98–105.
- 11 P. Hartmann, T. Leichtweiss, M. R. Busche, M. Schneider, M. Reich, J. Sann, P. Adelhelm and J. Janek, *J. Phys. Chem. C*, 2013, **117**, 21064–21074.
- 12 F. Han, T. Gao, Y. Zhu, K. J. Gaskell and C. Wang, *Adv. Mater.*, 2015, **27**, 3473–3483.
- 13 Y. Mo, S. P. Ong and G. Ceder, *Chem. Mater.*, 2012, **24**, 15–17.
- 14 Y. Zhu, X. He and Y. Mo, *ACS Appl. Mater. Interfaces*, 2015, **7**, 23685–23693.
- 15 A. Jain, G. Hautier, C. J. Moore, S. Ping Ong, C. C. Fischer, T. Mueller, K. A. Persson and G. Ceder, *Comput. Mater. Sci.*, 2011, **50**, 2295–2310.
- 16 A. Jain, G. Hautier, S. P. Ong, C. J. Moore, C. C. Fischer, K. A. Persson and G. Ceder, *Phys. Rev. B: Condens. Matter Mater. Phys.*, 2011, **84**, 045115.
- 17 L. Wang, T. Maxisch and G. Ceder, *Phys. Rev. B: Condens. Matter Mater. Phys.*, 2006, **73**, 195107.
- 18 K. Homma, M. Yonemura, T. Kobayashi, M. Nagao, M. Hirayama and R. Kanno, *Solid State Ionics*, 2011, **182**, 53–58.
- 19 R. Murugan, V. Thangadurai and W. Weppner, *Angew. Chem., Int. Ed.*, 2007, **46**, 7778–7781.
- 20 J. Awaka, A. Takashima, K. Kataoka, N. Kijima, Y. Idemoto and J. Akimoto, *Chem. Lett.*, 2011, **40**, 60–62.
- 21 S. Stramare, V. Thangadurai and W. Weppner, *Chem. Mater.*, 2003, **15**, 3974–3990.
- 22 J. L. Fourquet, H. Duroy and M. P. Crosnier-Lopez, *J. Solid State Chem.*, 1996, **127**, 283–294.
- 23 N. V. Kosova, E. T. Devyatkina, A. P. Stepanov and A. L. Buzlukov, *Ionics*, 2008, **14**, 303–311.
- 24 E. Dashjav and F. Tietz, *Z. Anorg. Allg. Chem.*, 2014, **640**, 3070–3073.
- 25 X. Yu, J. B. Bates, G. E. Jellison and F. X. Hart, *J. Electrochem. Soc.*, 1997, **144**, 524–532.

- 26 A. Jain, S. P. Ong, G. Hautier, W. Chen, W. D. Richards, S. Dacek, S. Cholia, D. Gunter, D. Skinner, G. Ceder and K. A. Persson, *APL Mater.*, 2013, **1**, 011002.
- 27 B. Fleutot, B. Pecquenard, H. Martinez, M. Letellier and A. Levasseur, *Solid State Ionics*, 2011, **186**, 29–36.
- 28 P. Knauth, *Solid State Ionics*, 2009, **180**, 911–916.
- 29 K. Senevirathne, C. S. Day, M. D. Gross, A. Lachgar and N. A. W. Holzwarth, *Solid State Ionics*, 2013, **233**, 95–101.
- 30 S. P. Ong, L. Wang, B. Kang and G. Ceder, *Chem. Mater.*, 2008, **20**, 1798–1807.
- 31 L. J. Miara, W. D. Richards, Y. E. Wang and G. Ceder, *Chem. Mater.*, 2015, **27**, 4040–4047.
- 32 C. H. Chen and K. Amine, *Solid State Ionics*, 2001, **144**, 51–57.
- 33 X. Xu, Z. Wen, X. Yang, J. Zhang and Z. Gu, *Solid State Ionics*, 2006, **177**, 2611–2615.
- 34 M. Kotobuki, H. Munakata, K. Kanamura, Y. Sato and T. Yoshida, *J. Electrochem. Soc.*, 2010, **157**, A1076–A1079.
- 35 J. Wolfenstine, J. L. Allen, J. Read and J. Sakamoto, *J. Mater. Sci.*, 2013, **48**, 5846–5851.
- 36 T. Hakari, M. Nagao, A. Hayashi and M. Tatsumisago, *J. Power Sources*, 2015, **293**, 721–725.
- 37 I. Kokal, M. Somer, P. H. L. Notten and H. T. Hintzen, *Solid State Ionics*, 2011, **185**, 42–46.
- 38 J. H. Woo, J. E. Trevey, A. S. Cavanagh, Y. S. Choi, S. C. Kim, S. M. George, K. H. Oh and S.-H. Lee, *J. Electrochem. Soc.*, 2012, **159**, A1120–A1124.
- 39 R. Ramachandran, M. Saranya, C. Santhosh, V. Velmurugan, B. P. C. Raghupathy, S. K. Jeong and A. N. Grace, *RSC Adv.*, 2014, **4**, 21151–21162.
- 40 K. Kishida, N. Wada, H. Adachi, K. Tanaka, H. Inui, C. Yada, Y. Iriyama and Z. Ogumi, *Acta Mater.*, 2007, **55**, 4713–4722.
- 41 T. Kato, M. Motoyama and Y. Iriyama, *Sintering Effects on the Resistivity of $\text{LiNi}_{1/3}\text{Mn}_{1/3}\text{Co}_{1/3}\text{O}_2$ /Ceramic-Solid-Electrolyte Interface in an All-Solid-State Battery*, Phoenix, AZ, USA, 2015.
- 42 T. Okumura, T. Nakatsutsumi, T. Ina, Y. Orikasa, H. Arai, T. Fukutsuka, Y. Iriyama, T. Uruga, H. Tanida and Y. Uchimoto, *J. Mater. Chem.*, 2011, **21**, 10051–10060.
- 43 H. Zhang, X. Liu, Y. Qi and V. Liu, *J. Alloys Compd.*, 2013, **577**, 57–63.
- 44 S. Jacke, J. Song, G. Cherkashinin, L. Dimesso and W. Jaegermann, *Ionics*, 2010, **16**, 769–775.
- 45 Y. Kim, G. M. Veith, J. Nanda, R. R. Unocic, M. Chi and N. J. Dudney, *Electrochim. Acta*, 2011, **56**, 6573–6580.
- 46 Y. Iriyama, T. Kako, C. Yada, T. Abe and Z. Ogumi, *J. Power Sources*, 2005, **146**, 745–748.
- 47 D. Ruzmetov, V. P. Oleshko, P. M. Haney, H. J. Lezec, K. Karki, K. H. Baloch, A. K. Agrawal, A. V. Davydov, S. Krylyuk, Y. Liu, J. Huang, M. Tanase, J. Cumings and A. A. Talin, *Nano Lett.*, 2012, **12**, 505–511.
- 48 N. J. Dudney, *Mater. Sci. Eng., B*, 2005, **116**, 245–249.
- 49 Y. Kobayashi, H. Miyashiro, K. Takei, H. Shigemura, M. Tabuchi, H. Kageyama and T. Iwahori, *J. Electrochem. Soc.*, 2003, **150**, A1577–A1582.
- 50 X. Li, R. Yang, B. Cheng, Q. Hao, H. Xu, J. Yang and Y. Qian, *Mater. Lett.*, 2012, **66**, 168–171.
- 51 H. G. Song, J. Y. Kim, K. T. Kim and Y. J. Park, *J. Power Sources*, 2011, **196**, 6847–6855.
- 52 Y. Wang, Ph.D. thesis, Michigan State University, 2014.
- 53 P. M. Raccach and J. B. Goodenough, *Phys. Rev.*, 1967, **155**, 932.
- 54 N. Ohta, K. Takada, L. Zhang, R. Ma, M. Osada and T. Sasaki, *Adv. Mater.*, 2006, **18**, 2226–2229.
- 55 H. Kitaura, A. Hayashi, K. Tadanaga and M. Tatsumisago, *Solid State Ionics*, 2011, **192**, 304–307.
- 56 K. Takada, N. Ohta, L. Zhang, K. Fukuda, I. Sakaguchi, R. Ma, M. Osada and T. Sasaki, *Solid State Ionics*, 2008, **179**, 1333–1337.
- 57 N. Ohta, K. Takada, I. Sakaguchi, L. Zhang, R. Ma, K. Fukuda, M. Osada and T. Sasaki, *Electrochem. Commun.*, 2007, **9**, 1486–1490.
- 58 T. Kato, T. Hamanaka, K. Yamamoto, T. Hirayama, F. Sagane, M. Motoyama and Y. Iriyama, *J. Power Sources*, 2014, **260**, 292–298.
- 59 A. Sakuda, H. Kitaura, A. Hayashi, K. Tadanaga and M. Tatsumisago, *Electrochem. Solid-State Lett.*, 2008, **11**, A1–A3.
- 60 Y. Jin, N. Li, C. H. Chen and S. Q. Wei, *Electrochem. Solid-State Lett.*, 2006, **9**, A273–A276.
- 61 B. D. McCloskey, R. Scheffler, A. Speidel, G. Girishkumar and A. C. Luntz, *J. Phys. Chem. C*, 2012, **116**, 23897–23905.
- 62 R. J. Bouchard, P. A. Russo and A. Wold, *Inorg. Chem.*, 1965, **4**, 685–688.
- 63 U. v. Alpen, A. Rabenau and G. H. Talat, *Appl. Phys. Lett.*, 1977, **30**, 621–623.
- 64 G. Nazri, *Solid State Ionics*, 1989, **34**, 97–102.
- 65 H.-J. Deiseroth, S.-T. Kong, H. Eckert, J. Vannahme, C. Reiner, T. Zaiß and M. Schlosser, *Angew. Chem., Int. Ed.*, 2008, **47**, 755–758.
- 66 E. Rangasamy, Z. Liu, M. Gobet, K. Pilar, G. Sahu, W. Zhou, H. Wu, S. Greenbaum and C. Liang, *J. Am. Chem. Soc.*, 2015, **137**, 1384–1387.
- 67 J. B. Goodenough and Y. Kim, *Chem. Mater.*, 2010, **22**, 587–603.
- 68 G. Hautier, S. P. Ong, A. Jain, C. J. Moore and G. Ceder, *Phys. Rev. B: Condens. Matter Mater. Phys.*, 2012, **85**, 155208.
- 69 Z. Liu, W. Fu, E. A. Payzant, X. Yu, Z. Wu, N. J. Dudney, J. Kiggans, K. Hong, A. J. Rondinone and C. Liang, *J. Am. Chem. Soc.*, 2013, **135**, 975–978.